



Essay

Study on Atomization and Dust Reduction Mechanisms of AEO-9-Charged Solution

Liyang Sun, Shaocheng Ge *, Xi Chen  and Shuo Liu 

College of Safety and Emergency Management Engineering, Taiyuan University of Technology, Taiyuan 030024, China

* Correspondence: geshaocheng@163.com; Tel.: +86-134-5315-6217

Abstract: To effectively improve the dust reduction rate of fine dust and prevent the occurrence of secondary dust, surfactant-charged water mist dust reduction technology is proposed. First, the water mist induction-charged atomization mechanism was perfected by an induction-charged spray experiment and the optimal atomization-charged voltage was determined to be 10 kV. Second, by surface tension and spray experiments on AEO-9-charged solutions, the lower the surface tension and viscosity of the solution, the better the atomization effect; the best atomization solution was 10 kV and 0.02% AEO-9. Finally, according to an electrostatic adsorption experiment, it was identified that there was an electrostatic interaction between coal dust and charged droplets. The contact angle experiment showed that the contact angle of the AEO-9 droplets decreased by 68.44% compared with water after 3 s of contact with coal dust. The wetting effect of bituminous coal was significantly improved by adding AEO-9 to water. A molecular simulation was used to study the molecular interaction mechanism among the H₂O, AEO-9, and bituminous coal molecules. The simulation results showed that AEO-9 was more active than water, it easily interacted with bituminous coal, and the hydrophilic group covered the surface of the bituminous coal molecules, which increased the electrostatic interaction between the water molecules and bituminous coal surface molecules. After adding AEO-9 to H₂O, the intermolecular interaction energy of the H₂O/AEO-9/bituminous coal system was enhanced more than that of the H₂O/bituminous coal system. This study provides the basis for the application of surfactant-charged water mist dust reduction technology.

Keywords: AEO-9-charged solution; spray droplet size; charged and atomization mechanism; molecular simulation; dust reduction mechanism



Citation: Sun, L.; Ge, S.; Chen, X.; Liu, S. Study on Atomization and Dust Reduction Mechanisms of AEO-9-Charged Solution. *Energies* **2023**, *16*, 2800. <https://doi.org/10.3390/en16062800>

Academic Editors: Mohammad Mahmudur Rahman, Dibyendu Sarkar, Rupali Datta and Prafulla Kumar Sahoo

Received: 25 February 2023

Revised: 13 March 2023

Accepted: 15 March 2023

Published: 17 March 2023



Copyright: © 2023 by the authors. Licensee MDPI, Basel, Switzerland. This article is an open access article distributed under the terms and conditions of the Creative Commons Attribution (CC BY) license (<https://creativecommons.org/licenses/by/4.0/>).

1. Introduction

China is the largest coal producer in the world. Coal plays a major role in the country's energy consumption structure, but the dust pollution caused by the process of coal mining is a serious concern [1–3]. Currently, there is a high incidence rate of pneumoconiosis in China due to the presence of fine dust (PM_{2.5}) as the main source of pollution. Fine dust adsorbs toxic and harmful gases into the human body, which can cause pneumoconiosis [4–6].

Charged and surfactant sprays are the two main components used to reduce dust [7–10] by decreasing the surface tension of water and increasing the activity of water molecules [11,12]. However, there are many limitations involved in this technique. In the charged spray dust reduction technique, the collision landing of the charged water mist and coal dust results in the disappearance of the charge of the water mist. Upon air drying the system, the settled fine dust rises with the wind and causes secondary dust pollution. The surfactant spray dust reduction increases the interaction between the coal dust and water mist, but there is no electrostatic attraction between them, resulting in a low collision efficiency. Surfactant-charged water mist dust reduction technology can maintain an effective collision rate and prevent secondary dust.

In the field of charged spray dust reduction, Teng et al. studied the influence of charging voltage, dust air velocity, and dust concentration on the dust reduction effect

through experiments [8]. D’Addio et al. studied the adsorption of 100–450 nm ultrafine particles by employing free-falling charged droplets. The results showed that the collection efficiency of the charged droplets on ultrafine particles was very significant [13]. Carotenuto et al. analyzed the influence of contact time between mist droplets and dust particles, water consumption, relative velocity of water/gas, and droplet size on the droplet-charged dust reduction effect and developed a mathematical model for charged spray dust reduction [14]. In the field of surfactant spray dust reduction, Yan et al. performed chemical modifications on sodium alginate and selected an environment-friendly and economical surfactant with high water retention, appropriate viscosity, and good wettability [15]. Sun et al. used starch, methyl methacrylate, acrylamide, and a surfactant as raw materials to prepare a dust suppressant with good wind resistance and hardness [16]. Chang et al. studied the dust reduction efficiency of different surfactant solutions through a wind tunnel test [17]. Although there have been remarkable advancements in the field of charged spray and surfactant spray dust reduction techniques, the performance and mechanisms of dust reduction of the combination of the two technologies remain to be further studied.

In this study, a highly efficient and environment-friendly fatty alcohol polyoxyethylene ether (AEO-9) was selected as the surfactant. By comparing the droplet size and the growth rate at different distances and charged voltages in a water mist induction-charged spray experiment, the mechanism of water mist induction-charged atomization was improved and the optimal charging voltage was determined. The surface tension values of the AEO-9 solution at different concentrations were also measured by a contact angle measuring instrument. Based on the surface tension values, three concentrations of AEO-9 solution were selected for the spray experiment and compared with the spray droplet size to determine the optimal AEO-9 concentration. The optimal charged voltage and concentration were then selected to compare the droplet size and the growth rate of the charged water mist, AEO-9 water mist, and AEO-9-charged water mist at different distances, and the atomization mechanism of the AEO-9-charged water mist was proposed. Finally, the dust reduction mechanism was revealed through an electrostatic adsorption experiment of the coal dust and charged droplets, a contact angle experiment of the AEO-9 solution at different concentrations, and a molecular simulation of the orbital information, electrostatic potential, and intermolecular interaction energy in different systems.

2. Experiment and Simulation

2.1. Experiment Details

2.1.1. Materials and Instruments

In this study, the purity of AEO-9 was $\geq 99\%$, produced from Shandong Yousuo Chemical Technology Co., Ltd., Qingdao, Shandong, China. The experimental coal sample was obtained from Lingshi County, Jinzhong, China. The coal samples were obtained by crushing and sieving; the particle size of the coal dust was $\leq 74 \mu\text{m}$. The prepared coal dust was placed in a desiccator for storage.

The instruments and models used for the experiment are shown in Table 1.

Table 1. Experimental instruments and models.

Equipment Name	Model
Ball mill	GMJ-2
Vibrating screen	BZS—300 mm
Vacuum drying oven	101-00AS
Air compressor	1500-2
High-voltage electrostatic DC generator (—)	TD2202N50-2000-A03
Blender	ZH18T
Laser particle size analyzer	HELOS (H4116) and UNIVERSAL
Magnetic stirrer	SN-MS-H
Contact angle measuring instrument	SDC-350
Tableting machine	YP-15

2.1.2. Measurement of the Droplet Size of the Spray

To measure the fog droplet size, a fog droplet measurement platform was built, as shown in Figure 1.

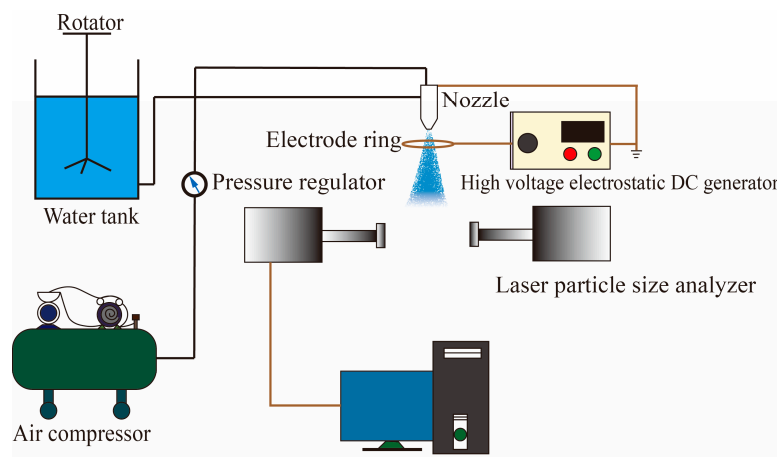


Figure 1. Schematic diagram of the experimental device.

It mainly included a water tank, rotator, air compressor, pressure regulator, siphon air atomization nozzle (grounded), electrode ring, high-voltage electrostatic DC generator (–), and laser particle size analyzer. The relevant parameters were set to 0.005%, 0.02%, and 0.04% mass concentration of the AEO-9 solution; 0.4 MPa atomization air pressure; 1 mm nozzle aperture (grounded); 50 mm electrode ring diameter; 5 kV, 10 kV, and 15 kV charged voltages; and 0.01 μm measurement accuracy of the laser particle size analyzer [18], which was characterized by the volume mean droplet (VMD) size. The measurement process was as follows: the AEO-9 solution was continuously stirred using a mixer, the air compressor was turned on, the water mist was ejected, the electrode ring was located in front of the nozzle and connected to a negative high-voltage electrostatic DC generator (grounded) to charge the water mist, and finally the water mist droplet sizes at 5 cm, 30 cm, 60 cm, 90 cm, and 120 cm away from the nozzle were measured by the laser particle size analyzer.

2.1.3. Measurement of the Surface Tension and Contact Angle

The AEO-9 solutions with mass concentrations of 0.005%, 0.007%, 0.01%, 0.02%, 0.03%, 0.04%, and 0.05% were taken, and their surface tension was determined using the contact angle measuring instrument. The measurement accuracy was 0.001 mN/m. We turned on the automatic liquid supply and surface tension measurement function, and the surface tension value of the solution was measured when the droplets broke up instantaneously. In addition, the surface tension and contact angle of the 0.02% AEO-9 and water solution were measured, and the measurement accuracy was 0.001°. First, the coal sheet was prepared in a tableting machine under a coal dust mass of 50 mg, pressure of 20 MPa, and time of 1 min. We then placed the prepared coal sheet on the workbench, adjusted the workbench and injector, and started the drip. When the droplets were about to fall, we opened the continuous shooting function to capture the instantaneous contact between the droplets and the coal sheet. The automatic fitting method was used to measure the contact angle of the coal dust.

2.1.4. Electrostatic Adsorption Experiment for Coal Dust and Charged Droplet

The experiment was performed using a contact angle measuring instrument and a negative high-voltage electrostatic DC generator. The negative high-voltage electrostatic DC generator was connected to the metal part of the syringe and grounded. The charged voltage was set to 3 kV. About 50 mg of coal dust was placed directly below the charged droplets. The distance between the charged droplets and coal dust was varied to observe the motion state.

2.2. Simulation Details

In this paper, a classical Wiser bituminous coal model [19,20] was used. The molecular structures of the bituminous coal and AEO-9 are presented in Figure 2.

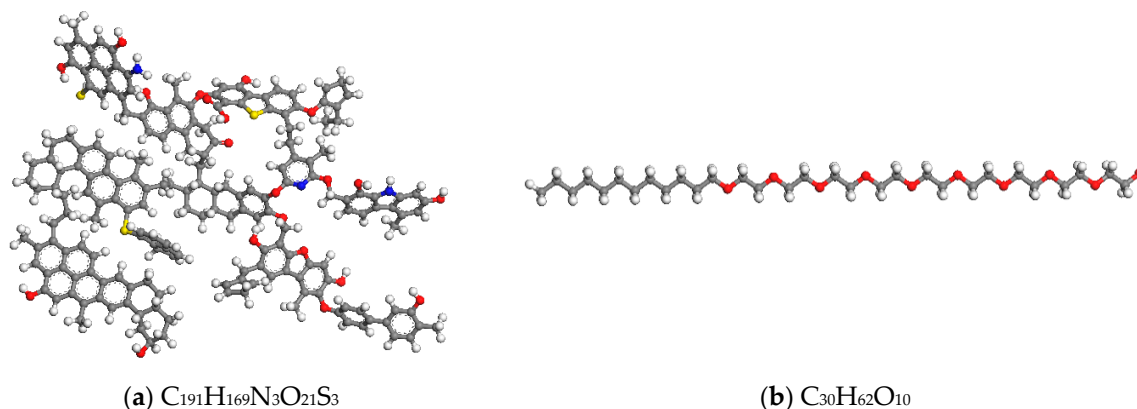


Figure 2. Molecular models: (a) bituminous coal; (b) AEO-9. The red, grey, white, yellow, and blue balls represent O, C, H, S, and N, respectively.

The HOMO orbital information, LOMO orbital information, and molecular surface electrostatic potential were obtained through a quantum mechanical simulation. The relevant parameters were set as follows: the module was Dom13, the task was geometry optimization, the quality was fine, the maximum iterations were 500, the functional was GGA, the employed method was BLYP, and the basis set was DNP.

The AC module was used to construct H_2O sphere, AEO-9, and bituminous coal molecule crystal models [21,22]. The water molecular density was set to 0.98 and the spherical diameter was set to 30 Å. The number of AEO-9 and bituminous coal molecules were 2 and 3, respectively. The build layer tool was then used to build the water/bituminous coal and water/AEO-9/bituminous coal models. The size of the models was 30 Å × 30 Å × 150 Å, as shown in Figure 3. First, the geometry optimization of the water/bituminous coal and the water/AEO-9/bituminous coal system was performed by the Forcite module, and the bond length, bond angle, and molecular configuration of the molecules in the systems were optimized. The relevant parameters were set as follows: the quality was ultrafine, maximum iterations were 50,000, the forcefield was compass II, the electrostatic summation method was Ewald, and the van der Waals summation method was Ewald. After optimization, a molecular dynamic simulation was performed under the relevant parameters mentioned as follows: the canonical ensemble (NVT) was selected, the thermostat was set as Nose, and the total simulation time was 1000 ps (the temperature and energy tended to be stable, and the systems had reached an equilibrium) [23].

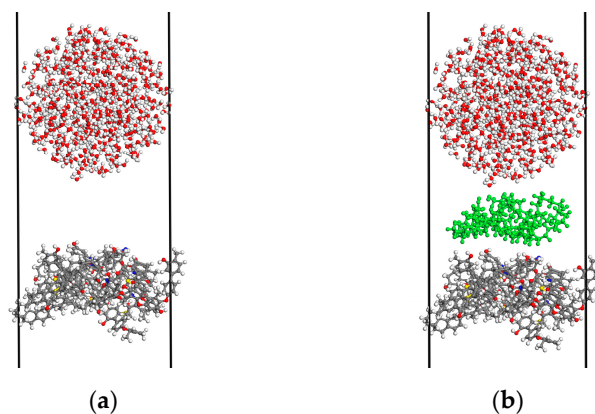


Figure 3. Different system models: (a) H_2O /bituminous coal; (b) H_2O /AEO-9/bituminous coal.

Although the molecular simulation conditions differed from the experimental conditions, the setting of the above two system parameters was the same. Therefore, by comparing the interaction energy of the two systems, the wetting properties and mechanism of the AEO-9 solution on bituminous coal could be qualitatively determined.

3. Results and Discussion

3.1. Water Mist Induction-Charged Atomization Mechanism

Figure 4 presents the water mist droplet size at different distances and charged voltages. At 0 kV and a 5 cm distance, the water mist droplet size was larger than it was at 5 kV and 10 kV. In the range of 30–120 cm, the droplet size of the water mist under 0 kV was less than that of the charged water mist. Based on former research [24] and the above results, the mechanism of the water mist-induced charged atomization was perfected, as shown in Figure 5. An electrode ring was placed directly below the nozzle, and an electric field was formed between the nozzle and the electrode ring [25]. According to the principle of induced charging, when the water mist was sprayed from the nozzle, a thick electric double layer was formed at the contact between the water and the nozzle. Under the action of the electrostatic field, the water mist carried positive charges, and the negative charges of the electric double layer were introduced into the earth from the nozzle. The water mist contained the same charges; thus, they repelled each other, leading to the breakup of the droplets. When the positive water mist passed through the negative electrode ring, there was a higher voltage difference between the electrode ring and the droplets. When the distance between the droplets and the electrode ring was small, the air was broken down and part of the droplets carried negative charges. After the water mist left the electrode ring, a large number of positive and negative charges remained within the system. With the increase in the distance, the droplets reunited under the action of static electricity and hydrogen bonding. The larger the growth rate of the spray droplets' size, the better the spray charging effect.

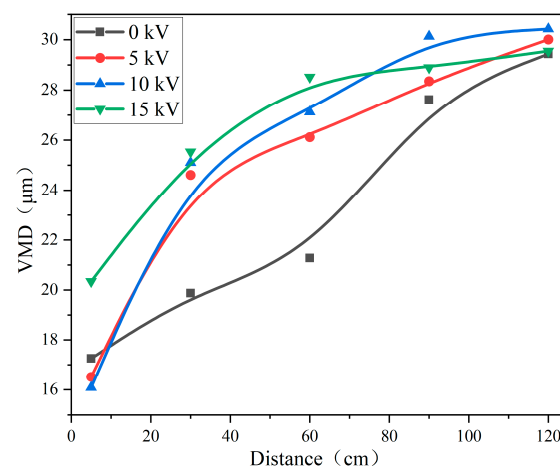


Figure 4. The water mist droplet size at different distances and charged voltages.

Figure 6 shows the growth rate of the spray droplets' size at different distances and charging voltages; the optimum charge voltage was 10 kV. With the increase in the induction-charged voltage, an optimal value was observed for the charged effect of the droplets because a corona discharge occurred after the voltage reached a certain value. The corona discharge was opposite to the charge of the induced charged spray droplets [18] and attracted each other. Therefore, the VMD was the largest at a distance of 5 cm and 15 kV.

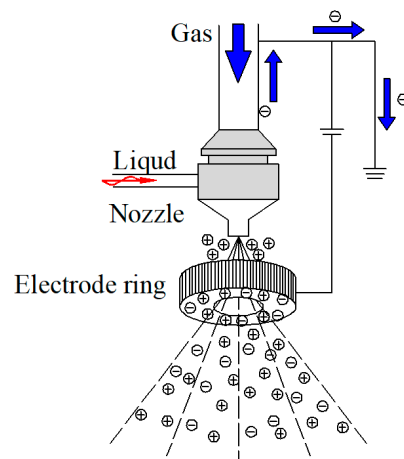


Figure 5. The water mist-induced charged atomization mechanism.

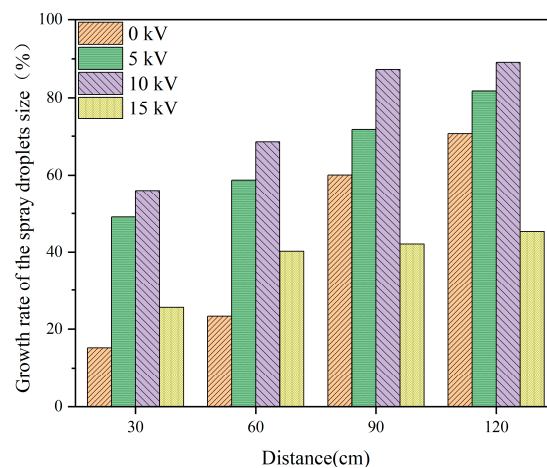


Figure 6. The growth rate of the spray droplets at different distances and charging voltages.

3.2. Atomization Mechanism of the AEO-9-Charged Solution

3.2.1. The Atomization Effect of the AEO-9 Solution

Figure 7 shows the surface tension of different concentrations of the AEO-9 solution. With the increase in concentration, the surface tension initially decreased and tended to stabilize when the concentration reached 0.02%, reaching a critical micelle concentration. Therefore, three concentrations—namely, 0.005%, 0.02%, and 0.04%—were selected for the spray experiments.

Figure 8 shows the spray droplet size of the AEO-9 solution with different concentrations and distances. The spray droplet size of 0.02% AEO-9 solution was the smallest. Although the surface tensions of 0.005% and 0.04% AEO-9 solutions were less than that of water, the viscosity was larger than that of water, which plays a major role, so the atomization effect of the water solution was better. Based on the above results, surface tension and viscosity together determined the atomization effect of the AEO-9 solution. In this study, the optimal atomization concentration of the AEO-9 solution was found to be 0.02%.

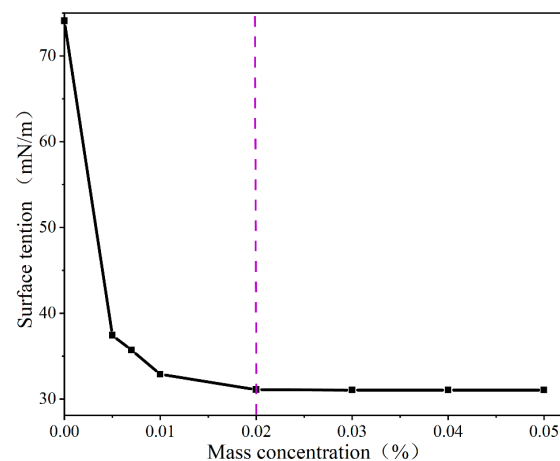


Figure 7. The surface tension of the AEO-9 solution at different concentrations.

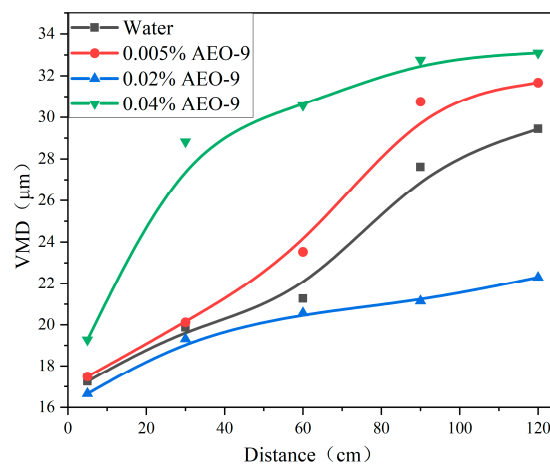


Figure 8. The spray droplet size of the AEO-9 solution at different concentrations.

3.2.2. Atomization Effect of the AEO-9-Charged Solution

Figure 9 shows the spray droplet size of 10 kV water, 0.02% AEO-9, and 10 kV and AEO-9 solutions. At 5 cm, the order of the spray droplet sizes of different solutions were 10 kV water < 10 kV and 0.02% AEO-9 < 0.02% AEO-9 because of the low viscosity and surface tension of 10 kV water (according to Figure 10). Figure 10 shows the surface tensions and shapes of 0.02% AEO-9 and water droplets at different charged voltages. With a further increase in the charged voltage, the surface tension of the droplets gradually decreased, resulting in the breakage of droplets. When the charged voltage was 10 kV, the AEO-9-charged droplets and water-charged droplets could not maintain their spherical shape and dripped continuously from the syringe. As the viscosity of water was relatively low, the droplet size was smaller. For 10 kV and 0.02% AEO-9 and 0.02% AEO-9 solutions, the viscosity was the same, but the surface tension of the former was lower (according to Figure 10), so the droplet size of 10 kV and 0.02% AEO-9 was slightly smaller.

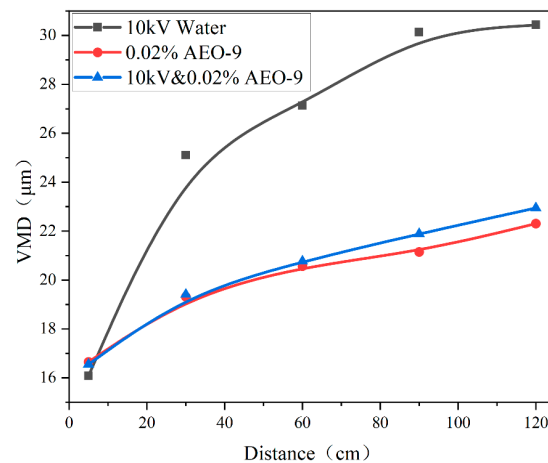


Figure 9. The water mist droplet size of 10 kV water, 0.02% AEO-9, and 10 kV and AEO-9.

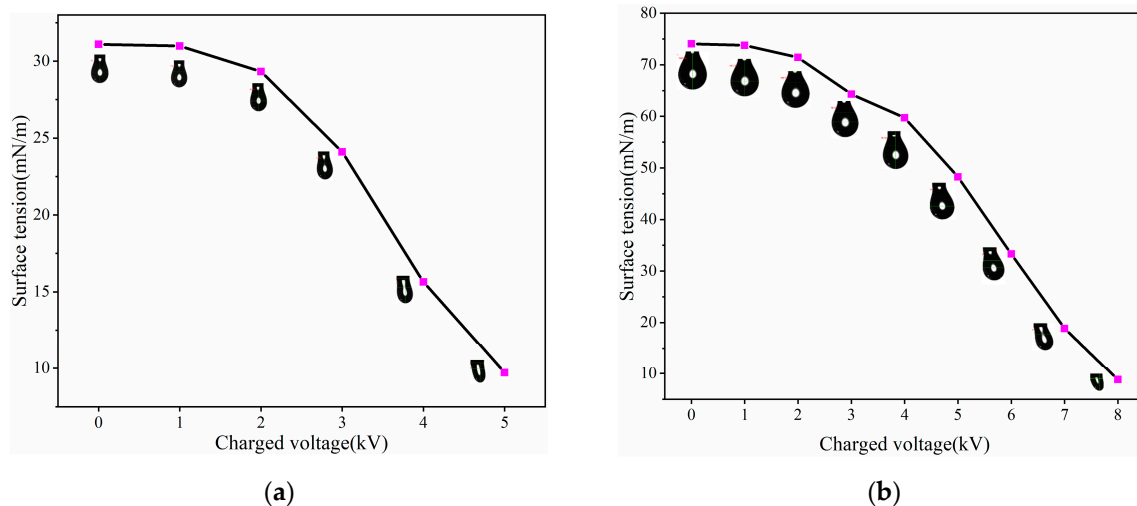


Figure 10. The surface tensions and shapes of droplets under different charged voltages: (a) 0.02% AEO-9-charged; (b) water-charged.

The droplets' reunion with the increase in distance and the growth rate of the spray droplet size is shown in Figure 11. Along 30–120 cm, the order of the droplets' reunion rate was 0.02% AEO-9 < 10 kV and 0.02% AEO-9 < 10 kV water. According to the water mist-induced charged principle as described in Section 3.1, more positive and negative charges accumulated in the spray with a higher spray droplet growth rate, and the better the charged effect. At 0–120 cm, considering the charged and atomization effect of the different solutions, the optimal solution was found to be 10 kV and 0.02% AEO-9.

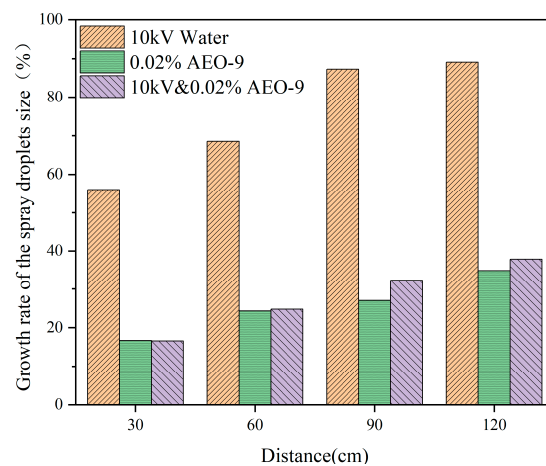


Figure 11. The droplet size growth rate of 10 kV water, 0.02% AEO-9, and 10 kV and 0.02% AEO-9.

3.3. Dust Reduction Mechanism of the AEO-9-Charged Solution

3.3.1. Electrostatic Adsorption Process

The schematic diagram of the interaction between 0.02% AEO-9-charged droplets and coal dust particles is given in Figure 12. As the distance between the coal dust particles and AEO-9-charged droplets decreased, the AEO-9-charged droplets gradually stretched and the electrostatic interaction between them was enhanced. This was mainly because the AEO-9-charged droplets induced positive and negative charges. As the distance between the droplets and coal dust particles decreased, the surface of the coal dust particles induced opposite charges under the action of mirroring force, increasing the electrostatic interaction between the two. The smaller the distance, the stronger the electrostatic interaction between the two. In summary, the AEO-9 solution was charged, increasing the dynamic collision probability between the coal dust particles and spray droplets.

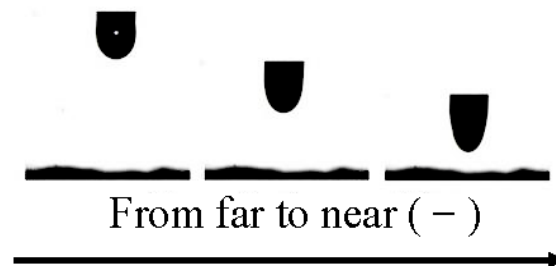


Figure 12. The interaction between the 0.02% AEO-9-charged droplets and coal dust particles.

3.3.2. Process and Contact Angle of Droplet-Wetting Coal Dust

After the combination of coal dust and charged droplets, the wettability of the droplets to coal dust determines the dust reduction efficiency. The contact angle is an important index to evaluate the wettability of a solution. The wettability is enhanced with a decrease in the contact angle [26,27]. Figure 13 is the wetting process and contact angle of water and 0.02% AEO-9 droplets to coal dust (time interval of 1 s). As the time changed, the droplets were slowly immersed in coal dust and the contact angle gradually decreased. After adding AEO-9 into the water, the contact angle decreased and the wettability increased.

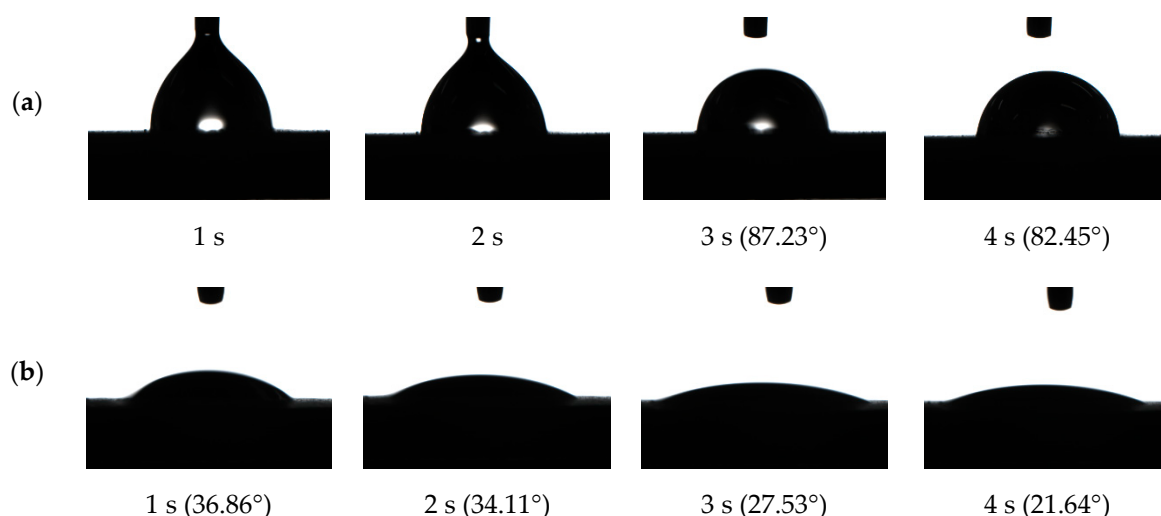


Figure 13. The wetting process and contact angle of the different solutions to coal dust: (a) water; (b) 0.02% AEO-9.

3.3.3. Front Orbital Analysis

The activities of the H₂O and AEO-9 molecules were determined by obtaining the energy values of the HOMO and LOMO orbitals. The HOMO occupies the highest energy and generally promotes the loss of electrons. As the energy of the HOMO level increases, the ability to lose electrons is enhanced. The LUMO occupies the lowest energy and usually accepts electrons. With the decrease in the energy of the LUMO level, there is an enhancement in the electron-accepting nature. The molecular activity becomes stronger with the decrease in the energy difference between the HOMO and LUMO levels [28,29]. Table 2 shows the HOMO and LOMO orbital energy information of the H₂O and AEO-9 molecules. AEO-9 showed a higher electron loss and electron acceptance capacity than H₂O. The difference between the two values of AEO-9 was less than H₂O. Therefore, the activity of AEO-9 was higher than that of H₂O, which effectively combined the bituminous coal molecules.

Table 2. HOMO and LOMO orbital energy values of H₂O and AEO-9 molecules.

Molecules	HOMO (Hartree/e)	LOMO (Hartree/e)	ΔE (Hartree/e)
H ₂ O	0.0313	−0.2458	0.2771
AEO-9	0.0173	−0.2049	0.2222

3.3.4. Electrostatic Potential Analysis

The electrostatic potential of molecules reflects the electrostatic interaction among them [23,30]. Figure 14 displays the electrostatic potential of the H₂O, AEO-9, and bituminous coal molecules. Table 3 shows the electrostatic potential values of the different molecules. The maximum positive potential of the bituminous coal was greater than that of H₂O, and the maximum negative potential was less than that of H₂O. The electrostatic attraction of H atoms connected with the O, N, and S atoms in the bituminous coal to the O atom in H₂O was greater than that of H atoms in H₂O, and the electrostatic attraction of O, N, S, and the benzene ring to the H atoms in H₂O was less than that of the O atom in H₂O. However, the proportion of H atoms connected to the O, N, and S atoms of the bituminous coal molecules was small, and the electrostatic effect between H₂O was stronger, leading to poor wettability of the water with the bituminous coal molecules.

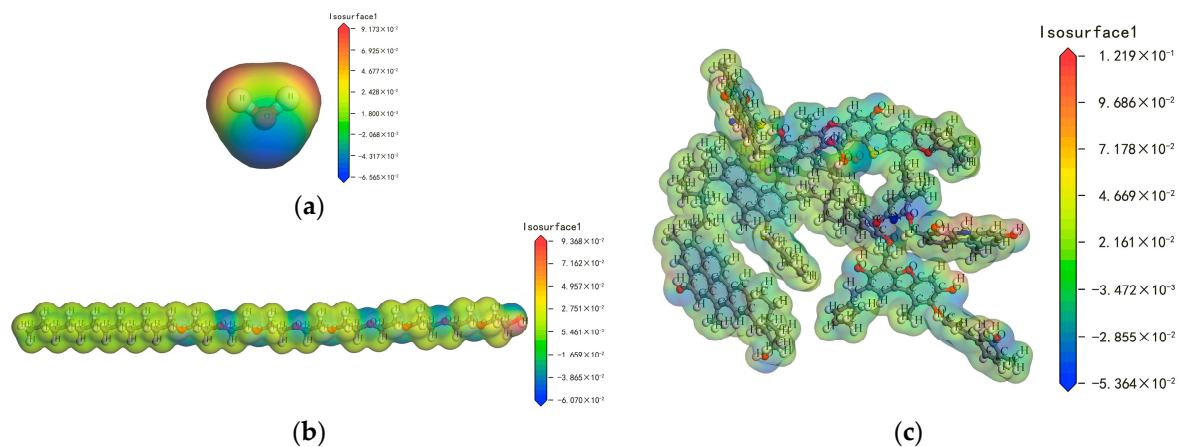


Figure 14. The electrostatic potential of different molecules: (a) H₂O; (b) AEO-9; (c) bituminous coal.

Table 3. The molecular electrostatic potential values of H₂O, AEO-9, and bituminous coal.

Molecules	Maximum Positive Potential (Hartree/e)	Location	Maximum Negative Potential (Hartree/e)	Location
H ₂ O	0.09173	Near H	−0.06565	Near O
AEO-9	0.09368	Near hydroxyl H	−0.0607	Near ether group and hydroxyl O
Bituminous coal	0.1219	Near H connected with O, N, and S	−0.05364	Near O, N, S, and the benzene ring

The addition of AEO-9 in water connected with the H₂O and bituminous coal molecules, changing the hydrophobicity of the bituminous coal. The maximum positive potential of AEO-9 was greater than that of H₂O, and the maximum negative potential was less than that of H₂O. The electrostatic attraction of the hydroxyl H atom in AEO-9 to the O atom in H₂O was greater than that of the H atoms in H₂O. The electrostatic attractions of the O atom in the ether and hydroxyl groups to the H atoms in H₂O were less than that of the O atom in H₂O. However, the number of H atoms in H₂O was greater than that of the O atom, so a part of the H₂O attracted the O atoms in the ether and hydroxyl groups of AEO-9, which caused the number of hydrogen bonds between the H₂O molecules to be reduced from 825 to 801. Therefore, the hydrogen bond interaction between the water molecules was weakened and the activity of the water molecules was enhanced. The corresponding electrostatic potential of the hydrophobic group in AEO-9 was near 5.461×10^{-3} Hartree/e. Under an electrostatic interaction, the hydrophobic groups were attached to the O, N, S, and benzene rings of the bituminous coal molecules.

3.3.5. Intermolecular Interaction Energy Analysis

The interaction energy characterizes the intermolecular interaction of the simulated system. The higher the interaction energy, the better the wettability of the coal dust [31,32]. In this paper, the potential energy was chosen to characterize the interaction energy of the simulation system, which was mainly composed of electrostatic and van der Waals energies. Table 4 displays the interaction energy of the different simulation systems. Upon the addition of AEO-9 to water, the electrostatic energy and van der Waals energy were increased between the water and bituminous coal molecules, and the wettability of the bituminous coal was improved.

Table 4. The interaction energy of different simulation systems.

System	Potential Energy (kcal/mol)	Electrostatic Energy (kcal/mol)	van der Waals Energy (kcal/mol)
H ₂ O/bituminous coal	−378.284	−286.405	−87.553
H ₂ O/AEO-9/bituminous coal	−499.718	−309.297	−186.757

4. Conclusions

The water mist induction charging mechanism was under the action of the electric field between the nozzle and the electrode ring. The water mist carried a large amount of positive charge, and the negative charges of the electric double layer flowed into the earth from the nozzle. When the water mist with a positive charge passed through the electrode ring with a negative charge, there was a high-voltage difference between the electrode ring and the water mist. The distance between the water mist and the electrode ring was small; under the action of the voltage difference, the air decomposed and part of the water mist had a negative charge. When the water mist left the electrode ring, the water mist contained a large number of positive and negative charges.

The droplet size of the AEO-9-charged solution decreased with the decrease in surface tension and viscosity of the solution. The optimal atomized solution was 10 kV and 0.02% AEO-9. As the spray distance increased, the AEO-9-charged droplets reunited under the action of electrostatic and hydrogen bonds, thus increasing the size of the droplets.

Compared with the water solution, the AEO-9-charged solution increased the electrostatic adsorption between the coal dust particles and droplets. It reduced the contact angle of the AEO-9 solution on the surface of the coal dust and increased the wettability of the coal dust.

The mechanism of the AEO-9 solution in improving the wettability of coal dust was revealed at a micro-level by a molecular simulation: the electron loss and electron-accepting ability of the AEO-9 molecule was higher than the H₂O molecule, which was effectively combined with the bituminous coal molecule. Under an electrostatic interaction between the H₂O and AEO-9 molecules, the number of hydrogen bonds between the H₂O molecules was reduced, resulting in the hydrogen bond interaction between the water molecules being weakened and the activity of the water molecules being enhanced. After AEO-9 was added to water, the electrostatic energy and van der Waals energy among the molecules in the system were enhanced, which improved the wetting ability of water on bituminous coal.

Author Contributions: Conceptualization, L.S., S.G. and S.L.; Methodology, L.S., S.G. and S.L.; Software, L.S. and S.L.; Validation, S.G. and X.C.; Formal Analysis, L.S.; Investigation, L.S.; Resources, L.S.; Data Curation, S.L.; Writing—Original Draft Preparation, L.S.; Writing—Review and Editing, S.G.; Visualization, L.S.; Supervision, S.G.; Project Administration, X.C.; Funding Acquisition, S.G. All authors have read and agreed to the published version of the manuscript.

Funding: This work was supported by the Transformation of Scientific and Technological Achievements Programs of Higher Education Institutions in Shanxi (grant number 2020CG022), the Youth Science Fund of the National Natural Science Foundation of China (grant number 51704145), and the Study on the Mechanism of Permeability and Wetting Improvement Induced By Sonic Blasting Fluctuating Activated Water Injection For Dust Suppression (grant number 52174195).

Data Availability Statement: The data from this study are available from the corresponding author upon request.

Conflicts of Interest: The authors declare no conflict of interest.

References

- Jing, D.; Jia, X.; Ge, S.; Zhang, T.; Ma, M. Numerical simulation and experimental study of vortex blowing suction dust control in a coal yard with multiple dust production points. *Powder Technol.* **2021**, *388*, 554–565. [\[CrossRef\]](#)
- Jing, D.; An, R.; Chen, J.; Ge, S.; Sun, L. Study on the Atomization and Dust-Reduction Performance of a New Type of External Pneumatic Vortex Fog Curtain Dust Removal Device in Fully Mechanized Excavation Face. *Adv. Mater. Sci. Eng.* **2020**, *2020*, 8356456. [\[CrossRef\]](#)
- Yang, L.; Ge, S.; Huang, Z.; Jing, D.; Chen, X. The influence of surfactant on the wettability of coal dust and dust reduction efficiency. *Arab. J. Geosci.* **2021**, *14*, 1336. [\[CrossRef\]](#)
- Li, B.; Yang, J.; Dong, H.; Li, M.; Cai, D.; Yang, Z.; Zhang, C.; Wang, H.; Hu, J.; Bergmann, S.; et al. PM_{2.5} constituents and mortality from a spectrum of causes in Guangzhou, China. *Ecotoxicol. Environ. Saf.* **2021**, *222*, 112498. [\[CrossRef\]](#)
- Li, Y.; Li, C.; Liu, J.; Meng, C.; Xu, C.; Liu, Z.; Wang, Q.; Liu, Y.; Han, J.; Xu, D. An association between PM_{2.5} and pediatric respiratory outpatient visits in four Chinese cities. *Chemosphere* **2021**, *280*, 130843. [\[CrossRef\]](#)
- Nirmalkar, J.; Haswani, D.; Singh, A.; Kumar, S.; Raman, R.S. Concentrations, transport characteristics, and health risks of PM_{2.5}-bound trace elements over a national park in central India. *J. Environ. Manag.* **2021**, *293*, 112904. [\[CrossRef\]](#)
- Shi, G.; Qi, J.; Wang, Y.; Liu, S. Experimental study on the prevention of coal mine dust with biological dust suppressant. *Powder Technol.* **2021**, *391*, 162–172. [\[CrossRef\]](#)
- Teng, C.; Li, J. Experimental Study on Particle Removal of a Wet Electrostatic Precipitator with Atomization of Charged Water Drops. *Energy Fuels* **2020**, *34*, 7257–7268. [\[CrossRef\]](#)
- Tessum, M.W.; Raynor, P.C. Effects of Spray Surfactant and Particle Charge on Respirable Coal Dust Capture. *Saf. Health Work.* **2017**, *8*, 296–305. [\[CrossRef\]](#)
- Zhou, L.; Yang, S.; Hu, B.; Yuan, Z.; Wu, H.; Yang, L. Evaluating the performance of a composite wetting dust suppressant on lignite dust. *Powder Technol.* **2018**, *339*, 882–893. [\[CrossRef\]](#)
- Zillgitt, M.; Schmidt, E. Determination of Operating Parameters for the Use of an Electrostatically Charged Water Spray Mist. *Chem. Eng. Technol.* **2021**, *44*, 1178–1184. [\[CrossRef\]](#)
- Yao, Q.; Xu, C.; Zhang, Y.; Zhou, G.; Zhang, S.; Wang, D. Micromechanism of coal dust wettability and its effect on the selection and development of dust suppressants. *Process. Saf. Environ. Prot.* **2017**, *111*, 726–732. [\[CrossRef\]](#)
- D'Addio, L.; Carotenuto, C.; Balachandran, W.; Lancia, A.; Di Natale, F. Experimental analysis on the capture of submicron particles (PM_{0.5}) by wet electrostatic scrubbing. *Chem. Eng. Sci.* **2014**, *106*, 222–230. [\[CrossRef\]](#)
- Carotenuto, C.; Di Natale, F.; Lancia, A. Wet electrostatic scrubbers for the abatement of submicronic particulate. *Chem. Eng. J.* **2010**, *165*, 35–45. [\[CrossRef\]](#)
- Yan, J.; Nie, W.; Zhang, H.; Xiu, Z.; Bao, Q.; Wang, H.; Jin, H.; Zhou, W. Synthesis and performance measurement of a modified polymer dust suppressant. *Adv. Powder Technol.* **2020**, *31*, 792–803. [\[CrossRef\]](#)
- Sun, J.; Zhou, G.; Gao, D.; Wei, Z.; Wang, N. Preparation and performance characterization of a composite dust suppressant for preventing secondary dust in underground mine roadways. *Chem. Eng. Res. Des.* **2020**, *156*, 195–208. [\[CrossRef\]](#)
- Chang, P.; Zhao, Z.; Xu, G.; Ghosh, A.; Huang, J.; Yang, T. Evaluation of the coal dust suppression efficiency of different surfactants: A factorial experiment. *Colloids Surf. A Physicochem. Eng. Asp.* **2020**, *595*, 124686. [\[CrossRef\]](#)
- Marchewicz, A.; Sobczyk, A.; Krupa, A.; Jaworek, A. Induction charging of water spray produced by pressure atomizer. *Int. J. Heat Mass Transf.* **2019**, *135*, 631–648. [\[CrossRef\]](#)
- Bertero, M.; Sedran, U. Conversion of pine sawdust bio-oil (raw and thermally processed) over equilibrium FCC catalysts. *Bioresour. Technol.* **2013**, *135*, 644–651. [\[CrossRef\]](#)
- Li, B.; Liu, S.; Fan, M.; Zhang, L. The effect of ethylene oxide groups in dodecyl ethoxyl ethers on low rank coal flotation: An experimental study and simulation. *Powder Technol.* **2018**, *344*, 684–692. [\[CrossRef\]](#)
- You, X.; He, M.; Zhu, X.; Wei, H.; Cao, X.; Wang, P.; Li, L. Influence of surfactant for improving dewatering of brown coal: A comparative experimental and MD simulation study. *Sep. Purif. Technol.* **2019**, *210*, 473–478. [\[CrossRef\]](#)
- Xu, C.; Wang, H.; Wang, D.; Zhu, X.; Zhu, Y.; Bai, X.; Yang, Q. Improvement of Foaming Ability of Surfactant Solutions by Water-Soluble Polymers: Experiment and Molecular Dynamics Simulation. *Polymers* **2020**, *12*, 571. [\[CrossRef\]](#) [\[PubMed\]](#)
- Niu, W.; Nie, W.; Yuan, M.; Bao, Q.; Zhou, W.; Yan, J.; Yu, F.; Liu, C.; Sun, N.; Xue, Q. Study of the microscopic mechanism of lauryl glucoside wetting coal dust: Environmental pollution prevention and control. *J. Hazard. Mater.* **2021**, *412*, 125223. [\[CrossRef\]](#) [\[PubMed\]](#)
- Wang, J.; Zhang, S.; Zuo, Z. Experimental Study of Influence Rules on Spray Charged Characteristics in the Induction Charging Process. *High Volt. Eng.* **2017**, *43*, 514–519.
- Xu, Y.-L.; Wang, L.-Y.; Yu, M.-G.; Wan, S.-J.; Song, Z.-P.; Wang, S.-K. Study on the characteristics of gas explosion affected by induction charged water mist in confined space. *J. Loss Prev. Process. Ind.* **2016**, *40*, 227–233. [\[CrossRef\]](#)
- Yuan, M.; Nie, W.; Zhou, W.; Yan, J.; Bao, Q.; Guo, C.; Tong, P.; Zhang, H.; Guo, L. Determining the effect of the non-ionic surfactant AEO9 on lignite adsorption and wetting via molecular dynamics (MD) simulation and experiment comparisons. *Fuel* **2020**, *278*, 118339. [\[CrossRef\]](#)
- Li, W.; Wang, H.; Li, X.; Liang, Y.; Wang, Y.; Zhang, H. Effect of mixed cationic/anionic surfactants on the low-rank coal wettability by an experimental and molecular dynamics simulation. *Fuel* **2020**, *289*, 119886. [\[CrossRef\]](#)

28. Martínez-Magadán, J.-M.; Oviedo-Roa, R.; García, P.; Martínez-Palou, R. DFT study of the interaction between ethanethiol and Fe-containing ionic liquids for desulfuration of natural gasoline. *Fuel Process Technol.* **2012**, *97*, 24–29. [[CrossRef](#)]
29. Israelachvili, J.N.; Adams, G.E. Direct measurement of long range forces between two mica surfaces in aqueous KNO₃ solutions. *Nature* **1976**, *262*, 774–776. [[CrossRef](#)]
30. Li, Y.; Zhou, G.; Li, J.; Gu, B.-L.; Duan, W. Alkali-Metal-Doped B₈₀ as High-Capacity Hydrogen Storage Media. *J. Phys. Chem. C* **2008**, *112*, 19268–19271. [[CrossRef](#)]
31. Zhang, Z.; Wang, C.; Yan, K. Adsorption of collectors on model surface of Wiser bituminous coal: A molecular dynamics simulation study. *Miner. Eng.* **2015**, *79*, 31–39. [[CrossRef](#)]
32. Guo, J.; Zhang, L.; Liu, S.; Li, B. Effects of hydrophilic groups of nonionic surfactants on the wettability of lignite surface: Molecular dynamics simulation and experimental study. *Fuel* **2018**, *231*, 449–457. [[CrossRef](#)]

Disclaimer/Publisher's Note: The statements, opinions and data contained in all publications are solely those of the individual author(s) and contributor(s) and not of MDPI and/or the editor(s). MDPI and/or the editor(s) disclaim responsibility for any injury to people or property resulting from any ideas, methods, instructions or products referred to in the content.